PART I

GENERAL SOLAR ACTIVITY, CORONAL HOLES AND BRIGHT POINTS

https://doi.org/10.1017/S0074180900071497 Published online by Cambridge University Press

EUV OBSERVATIONS OF THE ACTIVE SUN FROM THE HARVARD EXPERIMENT ON ATM

R. W. NOYES, P. V. FOUKAL, M. C. E. HUBER*, E. M. REEVES,
E. J. SCHMAHL, J. G. TIMOTHY, J. E. VERNAZZA, and G. L. WITHBROE

Center for Astrophysics, Harvard College Observatory and
Smithsonian Astrophysical Observatory, Cambridge, Mass. 02138, U.S.A.

Abstract. In this paper we review some preliminary results from the Harvard College Observatory Extreme Ultraviolet Spectroheliometer on ATM that pertain to solar activity. The results reviewed here are described in more detail in other papers referred to in the text. In the following paragraphs we first describe the instrument and its capabilities, and then turn to results on active regions, sunspots, flares, EUV bright points, coronal holes, and prominences.

I. The Instrument

The HCO scanning spectroheliometer consists of an 18-cm f/12.5 off-axis paraboloid feeding a normal-incidence concave grating spectrometer through a 5″-square entrance aperture. Seven detectors, located in the spectrometer focal plane, simultaneously record emission from a variety of wavelengths in the range 300 Å to 1335 Å. In the 'polychromatic' position of the grating, the seven wavelengths correspond to strong emission lines or continua ranging in temperature of formation from 10^4 K to 1.6×10^6 K, and other emission features can be selected by repositioning the grating. After the grating position is selected, the imaging mirror can perform a two-dimensional raster in angle, building up a set of simultaneous spectroheliograms each covering a 5′-square area with 5″ resolution. The time required to perform such a raster is 5.5 min. Alternatively, a one-dimensional scan, covering a region 5′ long but only 5″ wide, may be performed in 5.5 s, thus allowing data with high time resolution to be obtained for flares and other transient phenomena. A third observational mode is to fix the imaging mirror and position the ATM so that a solar feature of interest lies on the entrance slit, and rotate the grating continuously to build up a spectrum of the feature over the region 300–1335 Å with 1.5 Å spectral resolution and 3.3 min temporal resolution. For more details on the experiment and its capabilities see Reeves *et al.* (1974).

II. Active Regions

The HCO EUV observations of active regions are valuable because they can be used to study simultaneously the chromospheric and coronal layers where many solar transient phenomena occur. Figure 1 shows spectroheliograms constructed from digital data using a computer-driven cathode-ray tube display. Two active regions near the east limb are visible in these pictures, which illustrate how dramatically the

* On leave from ETH, Zürich, Switzerland.

Sharad R. Kane (ed.), Solar Gamma-, X-, and EUV Radiation, 3–17.

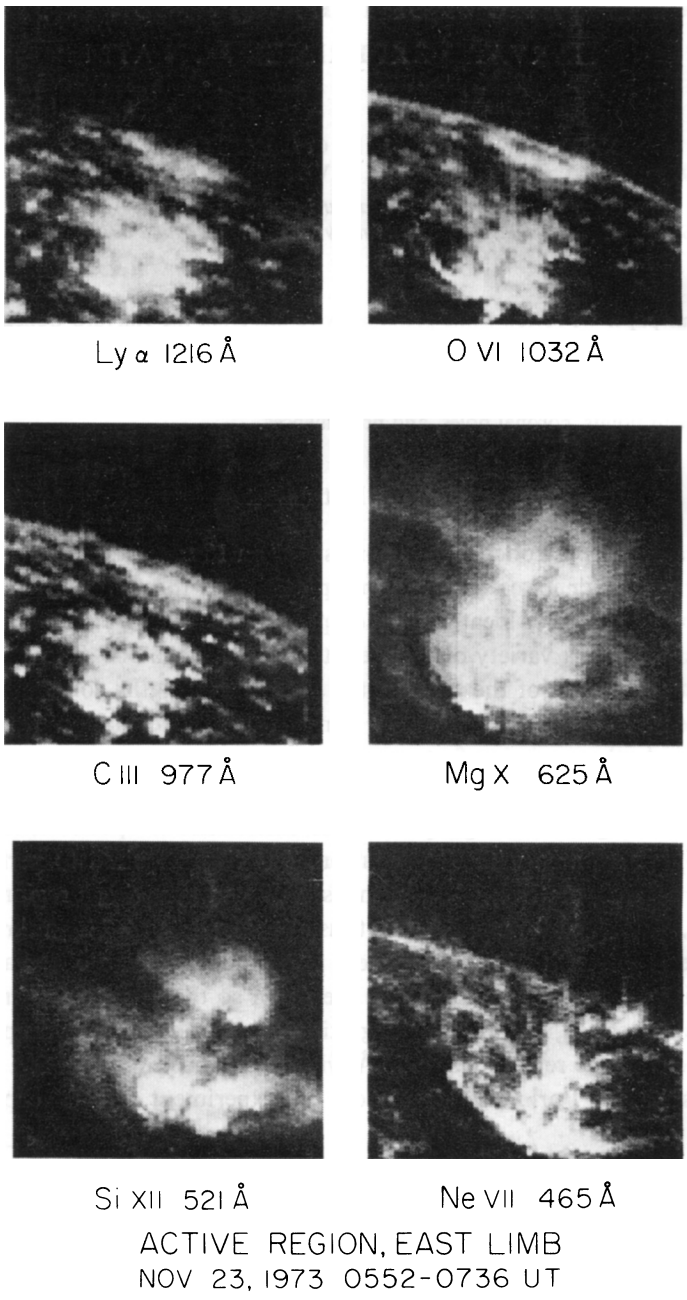

Fig. 1. Active region near the limb, viewed by the HCO instrument in its 'polychromatic' grating position. Images cover 5′ square, with 5″ spatial resolution, and are gray-level equivalents of the original digital data.

https://doi.org/10.1017/S0074180900071497 Published online by Cambridge University Press

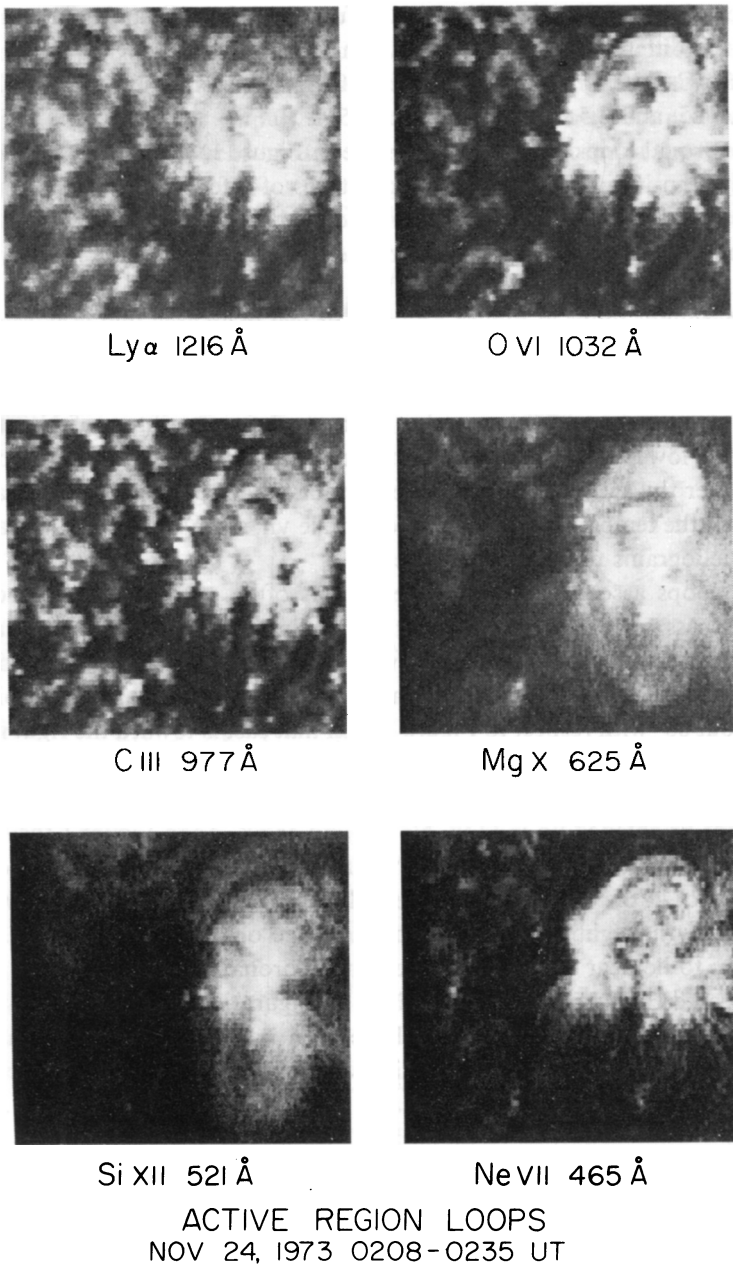

Fig. 2. Same active region viewed 18 h later, showing the development of loop structures.

https://doi.org/10.1017/S0074180900071497 Published online by Cambridge University Press

appearance of an active region changes as a function of temperature. The temperatures at which the different lines are most strongly emitted are 2×10^4 K for Lα λ1216, 8×10^4 K for C III λ977, 3×10^5 K for O VI λ1032, 6×10^5 K for Ne VII λ465, 1.5×10^6 K for Mg X λ625, and 2.5×10^6 K for Si XII λ521.

Several coronal loops or arches are visible in Figure 1. Generally these features are most easily seen in lines formed at temperatures of a few hundred thousand degrees and higher. Loops observed in lines formed between 10^5 K and 10^6 K are usually sharper and have higher contrast than the loops seen in lines formed at higher temperatures.

The foregrounds loops in Figure 1 have their feet in an area that is extremely bright in Ne VII λ465. That area lies over and adjacent to a large sunspot, the leading sunspot in the foreground active region. The following sunspot also appears to be marked by bright Ne VII emission, in this case by a large column or plume of Ne VII emission visible in the lower center of the Ne VII spectroheliogram. This column of material remained over the active region for several hours and must have a temperature close to 6×10^5 K, the temperature of formation of Ne VII, since the feature is nearly absent in spectroheliograms made in other lines.

Coronal loops associated with active regions often exhibit significant changes in EUV brightness on time scales ranging from minutes to hours. These changes may or may not be associated with flare activity. Figure 2 illustrates how the loops in the region in the foreground of Figure 1 had changed in about 18 h. These pictures are rotated about 60° with respect to Figure 1 such that east is toward the right in Figure 2 and toward the upper right corner of the pictures in Figure 1. The series of loops on the southern side of the active region (toward the left in Figure 1 and the top of Figure 2) has brightened up in O VI, Ne VII, and Mg X. As in Figure 1 the feet of the loops are located in an area bright in Ne VII that lies over and adjacent to the large leading sunspot in the active region. The following sunspot is located below the small dark area near the right (eastern) side of the plage observed in C III λ977. This spot also appears to lie near the feet of some of the coronal loops.

The increased EUV brightness of the loop configuration on the southern side of the active region as seen in Figure 2 may have been influenced by flares that occurred near the leader sunspot between the times of Figures 1 and 2, as described in a separate paper (Withbroe, 1975).

III. Flares

The HCO spectroheliometer has the capability to make observations of emission at several characteristic temperatures simultaneously, with high temporal resolution (5.5 s), and with high spatial resolution (5″) along a one-dimensional scan of 5′ length. By revealing the comparative behavior of the emission at different temperatures, such observations can restrict the range of possible mechanisms operative in the flare.

Preliminary analysis of such data (Noyes *et al.*, 1975) indicates that the impulsive rise in EUV emission occurs essentially simultaneously at all levels from the transition

zone to the corona, at least to within the 5.5 s resolution of the instrument. In many cases the simultaneous rise extends down to the Lα chromosphere, although in others (Figure 3) the chromospheric emission is delayed relative to the transition zone and coronal emissions and is not impulsive. However, two-dimensional rasters of flares (Withbroe, 1975) reveal that chromospheric flares tend to occur at the footpoints of

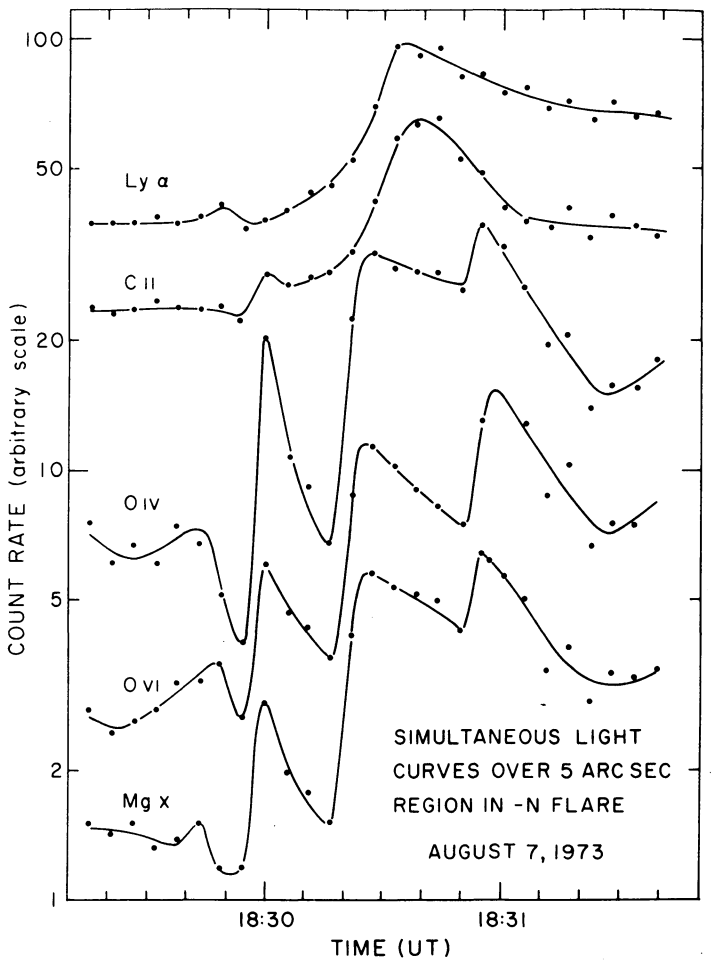

Fig. 3. Simultaneous light curves of a 5″ region in a small flare, showing impulsive brightening simultaneously in transition zone and corona, but time lags in the underlying chromosphere.

higher-temperature loops, which may be inclined to the vertical; therefore it seems possible that the lack of simultaneity in some of the high-time-resolution one-dimensional scans results from the scan slightly missing the chromospheric footpoint.

The rise time of impulsive emission in flares at all levels has been observed to be quite rapid, often with *e*-folding time shorter than the 5.5 s time resolution of the instrument.

https://doi.org/10.1017/S0074180900071497 Published online by Cambridge University Press

As expected, the maximum EUV intensity of flares, when averaged over the 5″ entrance slit of the ATM instrument, is higher than previous measurements using instruments with poorer spatial resolution that were less able to isolate the peak flare emission. In fact, for many flares the ATM instrument either saturated or tripped out when observing strong emission lines. From a spectrum near the peak of a small flare we obtain preliminary intensities (subject to slight modification when the final instrument calibration is available) as shown in Table I.

TABLE I

Intensities near maximum of 1 N flare, 1973 Sept. 2, 0236 UT, averaged over 5″ scan aperture

Line	T_{max}[a]	I_{flare}[b] (erg cm^{-2} s^{-1} sterad^{-1})	I_{quiet}[c] (erg cm^{-2} s^{-1} sterad^{-1})	I_{flare}/I_{quiet}
Lα	2×10^4	$>7.5\times10^5$	64000	>12
Lβ	2×10^4	2×10^5	730	270
LC, integrated	8×10^3	1×10^6	4000	250
N III 991	1×10^5	1.44×10^5	56	2500
O VI 1032	3×10^5	$>3.3\times10^5$	330	>1000
O V 760	2×10^5	4.4×10^4	44	1000
O V 630	2×10^5	6.7×10^4	525	125
Mg X 625	1.6×10^6	6.5×10^3	30	200
Fe XVI 335	3×10^6	1.0×10^5	<600	>160

[a] Approximate temperature of maximum emission in non-flaring Sun.
[b] Spectral scan, 1973 Sept. 2, 0235 UT, using preflight intensity calibration.
[c] Spectral scan, disk center, 1973 Aug. 31, 1313 UT, using preflight intensity calibration.

The data in Table I are only illustrative of flare intensities seen within a restricted 5″ aperture, since their relative values vary considerably from flare to flare (Noyes *et al.*, 1975).

The two O V lines have been included in Table I because their ratio is density-sensitive, and the greater enhancement of O V 760 over O V 630 in the flare is indicative of a large increase of density at a temperature of 200 000 K in the flare plasma. Calculations of Munro (1973) place the density well in excess of 10^{11} cm^{-3} although uncertainties in atomic data as well as the assumption of a statistically steady population of the O V energy levels prevent the assignment of a precise value.

The higher chromospheric densities in the flare plasma have an interesting effect on the hydrogen Lyman continuum emission spectrum (Noyes *et al.*, 1975). The slope and intensity of the continuum show it to be emitted nearly under LTE conditions (i.e., the high density drives the ground-state departure coefficient b_1 nearly to unity), although the electron temperature at optical depth unity in the Lyman continuum remains nearly unchanged from the quiet Sun value.

Localized flare brightenings, although seen simultaneously in lines with characteristic temperatures from chromospheric to coronal, are often followed by brightening in chromospheric and transition zone lines that move upward along pre-existing active region loops. This is suggestive of the ejection of chromospheric material into

the loop structures (Withbroe, 1975). It is clear from the ATM data that flares are intimately connected with overlying coronal loop structures, and that a full empirical understanding of the interaction requires simultaneous data in several lines over a two-dimensional field with high temporal and spatial resolution.

IV. Sunspots

HCO observations of sunspots (Foukal *et al.*, 1974) reveal a very intense emission in transition zone lines (2×10^5 K $< T_{max} < 5 \times 10^5$ K, where T_{max} is the temperature of maximum relative abundance of the ion in question). The enhancement may reach an order of magnitude above that of the surrounding plage region, although it is generally unremarkable for chromospheric or coronal lines. Figure 4 shows a set of EUV

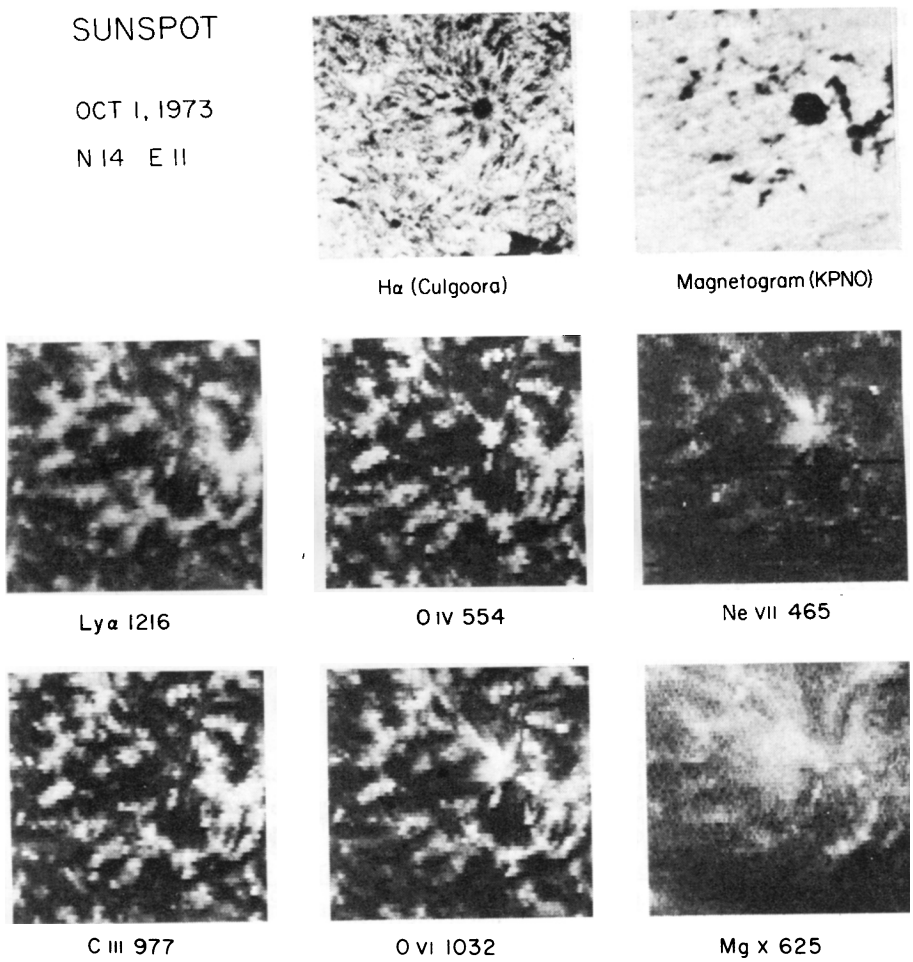

Fig. 4. Sunspot observed near disk center, showing the very large enhancement of lines formed between 2×10^5 K and 8×10^5 K.

https://doi.org/10.1017/S0074180900071497 Published online by Cambridge University Press

rasters over an isolated sunspot near disk center, in which very strong emission from transition zone lines appears directly over the sunspot umbra. In order of increasing temperature of formation, the remarkably strong emission first appears in O IV and other lines formed around 2×10^5 K; the emission is very localized, to a region centered on, and smaller than, the photospheric umbra. The halfwidth of the emission is seen in Figure 3 to increase regularly with height throughout the transition region, probably reflecting the fact that the magnetic field is diverging with height above the umbra.

The EUV spectrum of sunspots (Noyes, 1975) is remarkable, showing great enhancements of lines of N IV, V, O IV, V, VI, Ne IV, V, VI, VII, Mg VI, VII, VIII, and S IV, VI. In addition, intersystem lines of O V, Ne VI, and Ne VII are well-observed (Figure 5).

The very large transition zone emission above spots could be due to a localized increase of density in the transition zone, were it not for the fact that the intensity

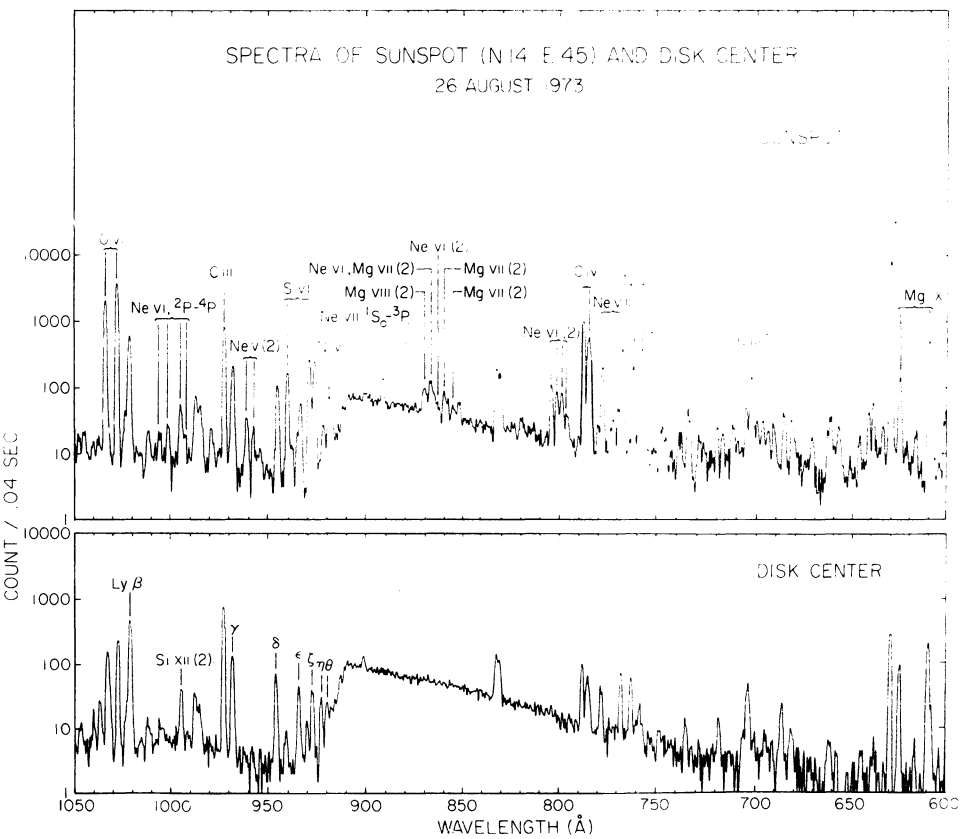

Fig. 5. Spectrum of 5″ region over sunspot umbra, showing very large enhancement of lines with characteristic temperatures between 200000 K and 800000 K. The Ne VI intersystem transitions near 1000 Å are seen for the first time in this spectrum.

https://doi.org/10.1017/S0074180900071497 Published online by Cambridge University Press

ratios of density-sensitive Be-like lines indicate if anything a *decrease* of density over that of the surrounding plage. A more reasonable interpretation is that the temperature gradient in the region 2×10^5 K $< T < 5 \times 10^5$ K above the umbra is decreased by up to an order of magnitude over that in the plage, thus increasing by a like factor the volume able to emit at a given temperature.

Although the intensity is enhanced by a factor of 10 in the transition zone over the umbra, the total emission is still negligible compared to the 'missing flux' from the photosphere in the spot umbra.

V. EUV Bright Points

Bright point sources of EUV radiation (Timothy *et al.*, 1975) have been observed in all locations on the disk. The sources can be most easily identified in Mg x 625.3 Å. Figure 6 shows a matrix of Mg x rasters covering the entire Sun, in which bright points appear to be uniformly distributed over the disk. Several hundred bright points, having dimensions of 30″ or less, can be seen in this image; many appear to be associated with bipolar magnetic-flux regions, based on an initial analysis of Kitt Peak National Observatory magnetograms taken on the same day (courtesy J. Harvey).

Bright points are most clearly observed in coronal holes (see Figure 7). Observations at the limb do not reveal any great differences in the apparent height of the peak of emission for Mg x 625.3 Å compared with that of H Lα 1215.7 Å. Consequently it is clear that the bright points do not extend to great distances in the corona and have a maximum altitude of the order of 1500 km or less. Some bright points are observed in transition region lines such as Ne VII 465.2 Å (see Figure 7), and yet are not visible in the coronal line Mg x 625.3 Å. Bright points which are clearly evident in transition region and chromospheric lines but invisible in coronal lines have also been observed outside of coronal holes. These points could represent a separate class of features or an earlier stage in the development of the bright points observed in coronal lines. A detailed analysis of the complete life history of a coronal bright point will be necessary to resolve this question.

No systematic differences have been observed in the emission from bright points inside and outside coronal holes. Many points appear as double features at transition region and chromospheric temperatures and as a laterally displaced single feature at coronal temperatures. This strongly suggests that a bright point has a basic loop structure.

Spectra of bright points for the wavelength range 1336 Å to 360 Å show an increase in the emission at all wavelengths of at least a factor of five compared with the average emission from a quiet region on the disk. Qualitatively, bright points appear to have a density about a factor of four greater than that of the surrounding medium, but show only a very small increase in temperature compared to that of the quiet corona.

A significant fraction of bright points exhibit flaring phenomena (Figure 8). Here the emission increases by an order of magnitude for a total lifetime of the order of that of a single raster scan (330 s). In at least one example the point has been observed

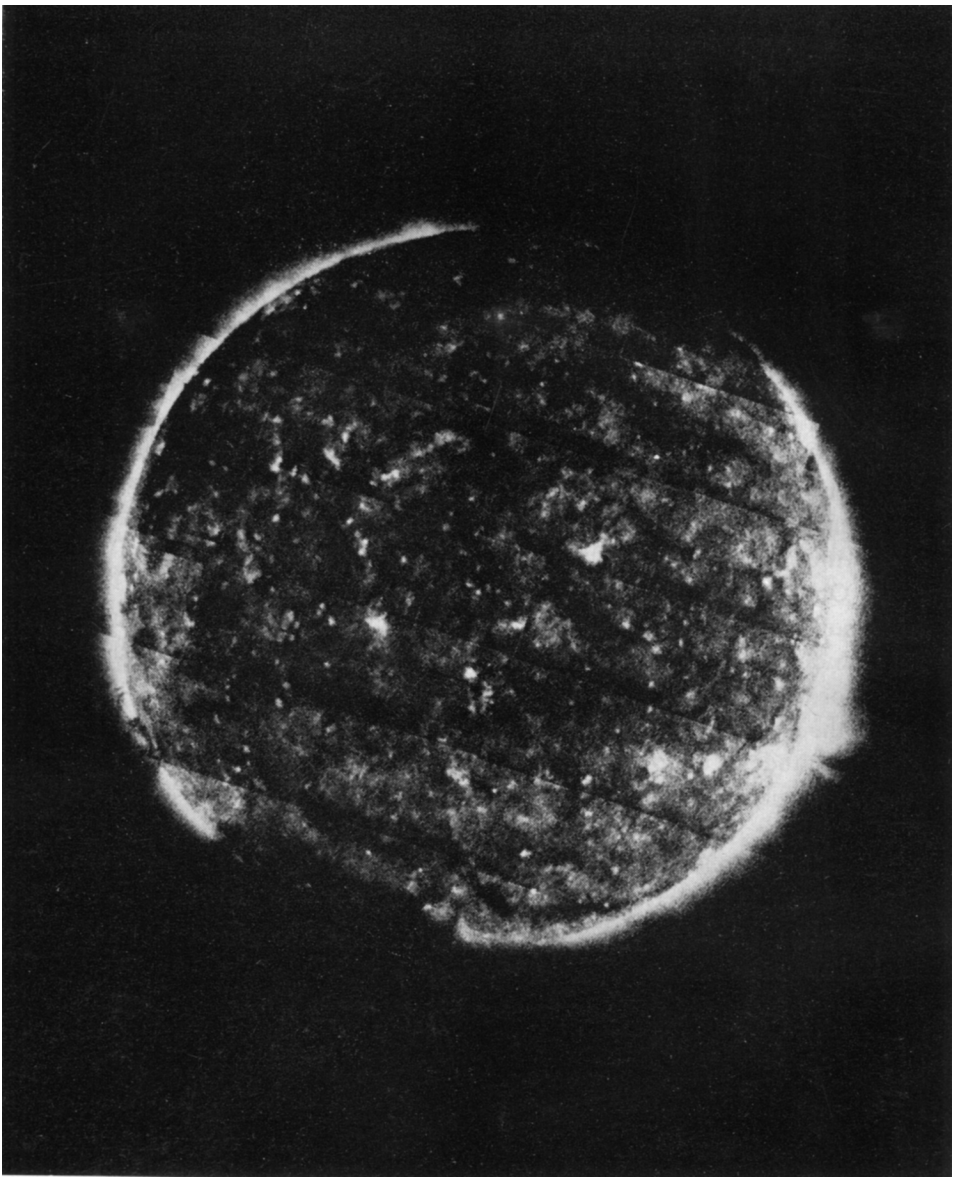

Fig. 6. EUV bright points seen in Mg x 625, in a matrix of 5′ rasters covering the entire solar disk, observed 28 January 1974. The banded structure is due to a defect in the plotting device.

to flare initially at transition region wavelengths. Furthermore, for a large fraction of flaring events a bright point several thousand kilometers away has been seen to flare simultaneously. No connecting loop structures between these regions have so far been observed.

https://doi.org/10.1017/S0074180900071497 Published online by Cambridge University Press

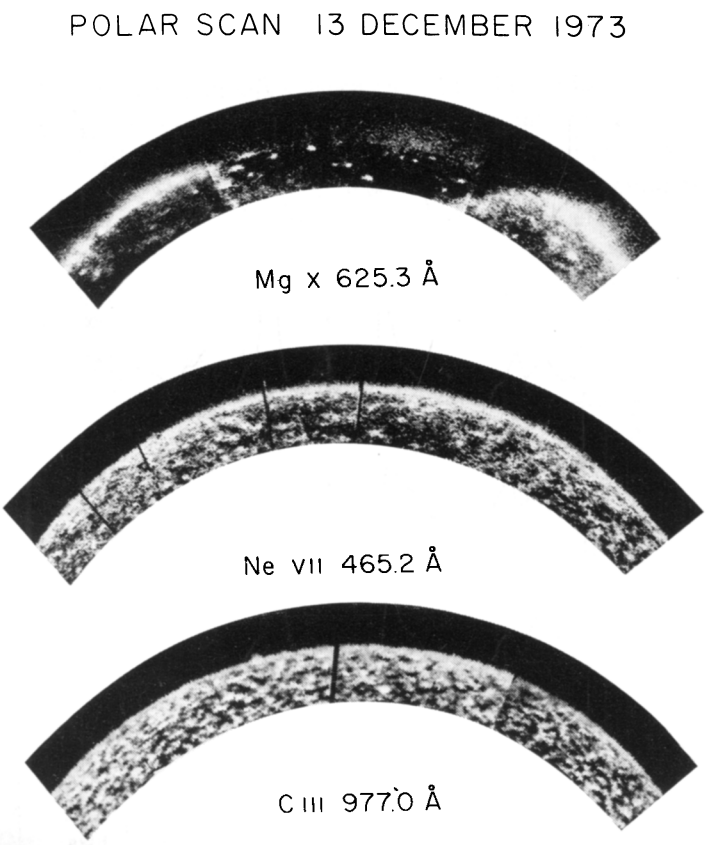

Fig. 7. Coronal hole at the south solar pole, showing EUV bright points in Mg x and a greater number in the transition zone line Ne VII.

We are now undertaking a detailed analysis of the structure of a series of bright points for which data have been recorded over the complete lifetime of several hours. These results will be correlated with X-ray and magnetic observations in order to produce a complete picture of the structure and energetics of these features in both the flare and the non-flare modes.

VI. Coronal Holes

Although coronal holes represent in one sense the antithesis of solar activity, their relevance for the overall structure of the general solar magnetic field and their apparent relation to the solar wind (Krieger *et al.*, 1973) are potentially important to several aspects of solar activity, so we include in this paper a short discussion of their properties as revealed by the HCO EUV data.

Coronal hole boundaries are obvious in coronal lines (Mg x 625 Å, for example) and are to some extent visible in lines formed above 7×10^5 K (e.g., Ne VIII, Ne VII). The ATM observations revealed that coronal holes actually manifest themselves in

https://doi.org/10.1017/S0074180900071497 Published online by Cambridge University Press

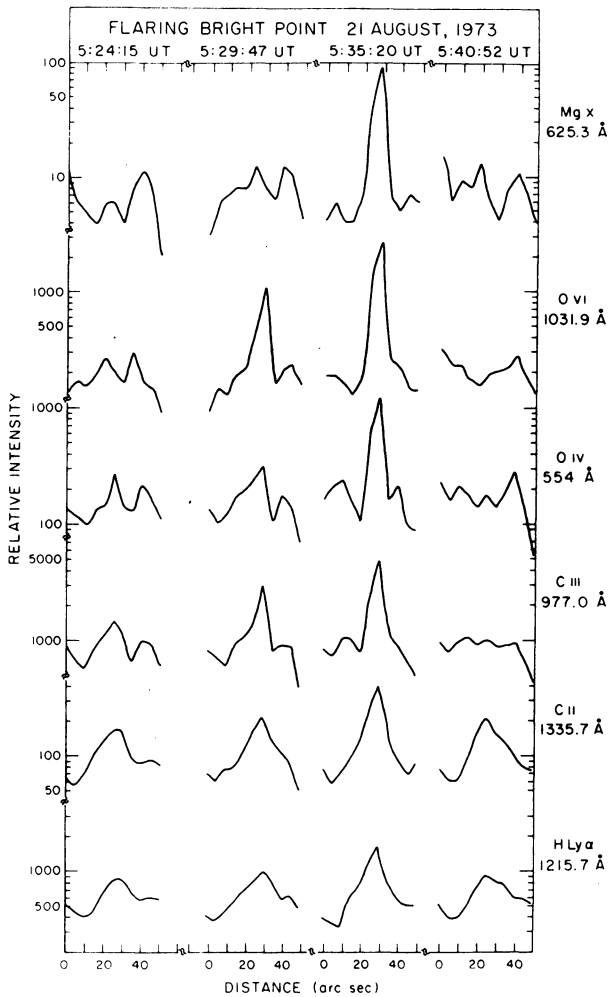

Fig. 8. Traces across flaring EUV bright point in four successive rasters in the polychromatic position. Note the early brightening in the transition zone.

all layers of the upper solar atmosphere (Huber *et al.*, 1974). In particular, the contrast between supergranulation boundaries and cells as seen in spectral features emitted by the chromosphere and transition zone is reduced inside coronal holes. The indications of lower density in the transition zone and chromosphere underlying coronal holes, as derived from the density-sensitive intensity ratio of the 1176 and 977 Å lines of C III (Munro and Withbroe, 1972) and from the color temperature of the Lyman continuum (Vernazza and Noyes, 1972), respectively, have been confirmed.

Furthermore, direct evidence for the resulting model having a thicker transition zone at the lower density inside holes (Munro and Withbroe, 1972) was obtained from limb observations of a polar coronal hole. Owing to the improved spatial resolution

available on the ATM instrument, we can directly observe the increased thickness of the transition zone as increased height of emission of transition zone lines. Figure 9 (Huber *et al.*, 1974) shows measured displacements of the limb above the polar coronal hole of Figure 7, relative to the nearby quiet atmosphere outside the hole. From this result we infer a reduction of downward thermal conduction in the hole by a factor of about six relative to the quiet Sun, in agreement with the earlier findings of Munro and Withbroe (1972).

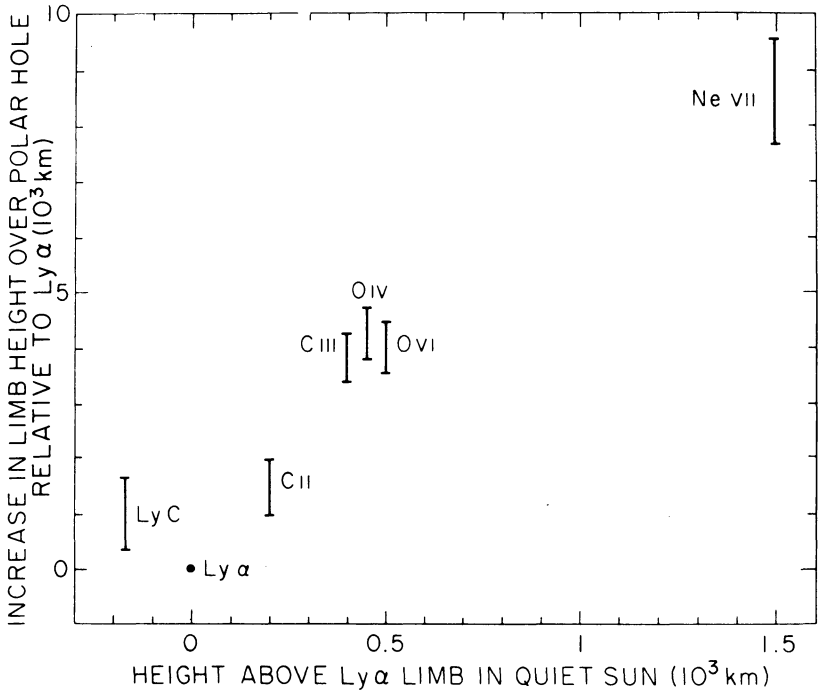

Fig. 9. Increase in limb height of various lines over coronal hole of Figure 7, compared with nearby quiet limb.

VII. Prominences

HCO observations of quiescent prominences (Schmahl *et al.*, 1974) include spectroheliograms in the strong lines and continua of hydrogen and helium, by means of which the cool threads of prominences and filaments absorb and radiate most of their energy. In addition the data include spectroheliograms of many important lines radiated by the transition sheath between the threads and the surrounding corona. Prominences appear to have a cold central core ($\sim$6000–7000 K) surrounded by a thin transition zone which merges with the hot corona (Noyes *et al.*, 1972) analogous to the temperature profile of the normal chromosphere, transition zone, and corona. This similarity makes it possible to derive properties of prominences by comparisons of line intensities in prominences and in the quiet solar atmosphere.

https://doi.org/10.1017/S0074180900071497 Published online by Cambridge University Press

When prominences are observed near the limb in Lα and the Lyman continuum, the limb is entirely obscured by the prominence. This implies that prominences are optically thick at these wavelengths, in agreement with theoretical expectations (Hirayama, 1964). Furthermore, the 5″ slit is filled by the emitting material. Simultaneous spectroheliograms at two wavelengths in the Lyman continuum determine a color temperature of the emitting hydrogen. This temperature lies between 5500 and 8000 K, with the lower values tending to occur near the middle and the higher values near the edges and top of prominences. This result confirms earlier, lower resolution EUV data (Noyes *et al.*, 1972).

From the color temperature and the intensity of the Lyman continuum, we can determine the departure coefficient b_1 for the ground state of hydrogen. We expect b_1 to be of the order of unity since the kinetic temperatures are comparable to the radiation temperature, and this indeed is the case.

All of the lines (exclusive of helium) emitted by the hotter portions of prominences are optically thin, for prominences appear transparent in these lines when they are observed against the solar disk. The optical depth of prominences can be determined by the relative brightnesses of the prominences against the limb, just above the limb, and the limb itself. (The filling of the slit can be guaranteed by the opaque appearance of the prominence in Lα or the Lyman continuum.) For C III λ977, the value of the optical depth ($\tau \approx 0.3$) is about half that found by Withbroe (1970) for the quiet transition zone. This implies that the column density of the C III-emitting prominence sheath (i.e., within the temperature range 5×10^4 K $\lesssim T \lesssim 1.2 \times 10^5$ K) is about half that of the quiet transition zone.

The thickness of the prominence transition sheath can be estimated from the ratio $\tau^2/I \propto (N_e\, dh)^2/N_e^2\, dh$. This result yields a thickness of about 10 km for the C III transition sheath on either side of the threads. In addition, by the slightly different technique of comparing the O VI emission in the prominence with that in the quiet corona off the limb, we can deduce a thickness of about 40 km on either side of the threads for the temperature range 2×10^5 K $\lesssim T \lesssim 5 \times 10^5$ K. Both of these determinations lead to a prominence transition zone thickness about a factor of two thinner than that for the quiet solar atmosphere (Dupree, 1972).

The thickness inferred above, when combined with the observed intensities, implies an electron density about half that at the same temperature in the quiet solar atmosphere. This is a surprising result, which is not clearly understood. It is worth noting that the density as inferred independently from the density-sensitive line ratio I(C III λ1176)/I(C III λ977) is also about half that of the quiet Sun at the same temperature.

The intensity of the optically thin lines formed at temperatures $> 2 \times 10^4$ K increases to a maximum near the top of prominences. This result suggests that the sheath thickness increases with height, or that the temperature gradient between the hydrogen threads and the corona decreases with height. A possible explanation is that the conductive flux inward from the corona is balanced locally by the radiative flux outward. Then, since the emissivity of the threads (as seen in the Lyman lines and the Lyman

continuum) is a decreasing function of height, the conductive flux inward must also decrease with height, and hence the sheath increases in thickness to accomplish this.

Much of the analysis for quiescent prominences may be extended to active loops and filaments, surges, and eruptive prominences. Work is progressing along these lines in the analysis of ATM data.

Acknowledgments

The results reported here reflect the long labors of very many individuals, without which there would be no results to report. The authors wish to express their gratitude for the wisdom, foresight, dedication, and courage of the NASA administrators, scientists, engineers, and astronauts who made Skylab the success it was. Portions of this work were supported through NASA contract NAS 5-3949.

References

Dupree, A. K.: 1972, *Astrophys. J.* **178**, 527.
Foukal, P. V., Huber, M. C. E., Noyes, R. W., Reeves, E. M., Schmahl, E. J., Timothy, J. G., Vernazza, J. E., and Withbroe, G. L.: 1974, *Astrophys. J. Letters* **193**, L 143.
Hirayama, J.: 1964, *Publ. Astron. Soc. Japan* **16**, 104.
Huber, M. C. E., Foukal, P. V., Noyes, R. W., Reeves, E. M., Schmahl, E. J., Timothy, J. G., Vernazza, J. E., and Withbroe, G. L.: 1974, *Astrophys. J. Letters* **194**, L 115.
Krieger, A. S., Timothy, A. F., and Roelof, E. C.: 1973, *Solar Phys.* **29**, 505.
Munro, R. H.: 1973, Thesis, Harvard University.
Munro, R. H. and Withbroe, G. L.: 1972, *Astrophys. J.* **176**, 511.
Noyes, R. W.: 1975, to be submitted to *Astrophys. J.*
Noyes, R. W., Dupree, A. K., Huber, M. C. E., Parkinson, W. H., Reeves, E. M., and Withbroe, G. L.: 1972, *Astrophys. J.* **178**, 515.
Noyes, R. W., Foukal, P. V., Huber, M. C. E., Reeves, E. M., Schmahl, E. J., Timothy, J. G., Vernazza, J. E., and Withbroe, G. L.: 1975, to be submitted to *Solar Phys.*
Reeves, E. M., Timothy, J. G., and Huber, M. C. E.: 1974, *Proc. S.P.I.E.* **44**, 159.
Schmahl, E. J., Foukal, P. V., Huber, M. C. E., Noyes, R. W., Reeves, E. M., Timothy, J. G., Vernazza, J. E., and Withbroe, G. L.: 1974, *Solar Phys.* **39**, 337.
Timothy, J. G., Foukal, P. V., Huber, M. C. E., Noyes, R. W., Reeves, E. M., Schmahl, E. J., Vernazza, J. E., and Withbroe, G. L.: 1975, to be submitted to *Solar Phys.*
Vernazza, J. E. and Noyes, R. W.: 1972, *Solar Phys.* **26**, 325.
Withbroe, G. L.: 1970, *Solar Phys.* **11**, 208.
Withbroe, G. L.: 1975, in preparation.